A Prototype Information System for Monitoring and Predicting Phytoplankton Productivity over Galveston Bay

2015-2017

GLO Contract No. 16-055-000-9099

A REPORT FUNDED BY A TEXAS COASTAL MANAGEMENT PROGRAM GRANT APPROVED BY THE TEXAS LAND COMMISSIONER PURSUANT TO NATIONAL OCEANIC AND ATMOSPHERIC ADMINISTRATION AWARD NO. NA15NOS4190162

Prepared by:

Drs. Huilin Gao[a] and Daniel Roelke[b]

[a]Texas A&M Engineering Experiment Station, College Station, TX 77843

[b]Dept. of Wildlife and Fisheries Sciences, Texas A& M University, College Station, TX 77843

Email: hgao@civil.tamu.edu

Phone: (979) 845-2875

Project Summary

Galveston Bay is among the largest bay systems in the western Gulf of Mexico, and is of significant economic, ecological, and recreational value. Coastal ecosystems rely heavily on phytoplankton production, which warrants having a near real-time platform to monitor variations in time and space across the entire bay. Phytoplankton productivity—represented by Chlorophyll-a concentration levels—is significantly affected by inflows from rivers (i.e. river discharges). Therefore, accurate inflow prediction is indispensable for projecting phytoplankton dynamics and composition, and maintaining ecosystem health. The prototype information system developed in this project contains two parts: a monitoring component, and a predicting component. The Chlorophyll-a concentration levels in the Galveston Bay were monitored using three satellite datasets: Landsat images, Moderate Resolution Imaging Spectroradiometer (MODIS) reflectance images, and Medium Resolution Imaging Spectrometer (MERIS) images. The prediction of phytoplankton productivity was conducted in three steps: (1) the Distributed Hydrology Soil Vegetation Model (DHSVM) was set up over the Trinity and San Jacinto River basins; (2) a long-term relationship between observed inflows and remotely sensed phytoplankton productivity was established; and (3) the model was then applied to conduct seasonal forecasting of phytoplankton driven by predicted seasonal weather forecasts from the National Centers for Environmental Prediction (NCEP) Climate Forecast System (CFS).

Education and outreach activities have been carried out in the form of advising graduate students, educating high school students, conducting workshops at various locations within the Galveston Bay area, presenting our methodology and results at professional conferences, and preparing peer-reviewed journal papers.

1. Introduction

Linking rivers with ocean environments, estuaries play an important role in aquatic ecosystem service and function. However, many U.S. estuaries are threatened by various environmental problems—such as water quality degradation, eutrophication, and fish resources decline. A study by Bricker et al. (2008) showed that around 84 out of 139 U.S. coastal areas had experienced eutrophication. With regard to water quality monitoring, an abnormally high chlorophyll a (Chlorophyll-a) concentration is usually considered as a reliable indicator of eutrophication. The spatial and temporal distributions of Chlorophyll-a can be greatly influenced by freshwater inflows, circulation, salinity, sediment loading, nutrients loading, and water temperature (Harding 1994). In addition, the seasonal-to-interannual variabilities of coastal Chlorophyll-a are also indirectly affected by anthropogenic influences (such as urbanization, agriculture, and population development) and climatic influences (Harding et al. 2016).

By transporting nutrients and sediments—as well as by altering estuary circulations—freshwater inflow plays a key role in algae growth, which significantly affects Chlorophyll-a concentration levels. Especially with the ongoing population growth, extensive urbanization, and increased wastewater discharge that many areas are experiencing—combined with climate change—both the timing and the magnitude of freshwater inflows have become more sensitive and capricious (Cloern *et al.* 2001; Roberts and Prince 2010; Camacho *et al.* 2015). A number of studies have investigated the impact of freshwater inflow on Chlorophyll-a concentrations in coastal areas. For instance, studies using observational data over the span of sixty years (1950-2010) in Chesapeake Bay found that wet years resulted in large inflow levels and high Chlorophyll-a concentrations, while dry years led to small inflows and low Chlorophyll-a concentrations in the bay (Harding 2016). Research resulting from aircraft remote sensing of ocean color also confirmed the view reported nearly 30 years ago that the magnitude of freshwater flows explained the inter-annual variability of

phytoplankton biomass (Malone *et al*. 1988; Miller and Harding 2007). In San Francisco Bay, an analysis of in-situ data by Cloern (1991) indicated a strong connection between the magnitude of annual spring algal blooms (during March-May) and the magnitude of the wet season (January through April) freshwater inflows. In Tampa Bay, Florida, a positive correlation between annual mean discharge and Chlorophyll-a was also revealed as well based on long-term observations from satellites (Le *et al.* 2013). In Perdido Bay, Florida, it was found that large inflows could promote algae growth by reducing the anoxia and hypoxia conditions in the bay (Xia and Jiang 2015). In other international estuaries similar positive correlations were identified—including in the Guadalquivir Estuary in Spain (Drake *et al.* 2002), the Loire River Estuary in France (Meybeck *et al.* 1988), and the Kasouga Estuary in South Africa (Froneman 2002).

Galveston Bay is among the largest bay systems in the western Gulf of Mexico, and is of significant economic, ecological, and recreational value for the State of Texas. Coastal ecosystems rely heavily on phytoplankton production, which warrants a near real-time platform to monitor variations in time and space across the entire bay. Phytoplankton productivity is significantly affected by inflows from rivers (i.e. river discharges). Therefore, accurate inflow prediction is indispensable for projecting phytoplankton dynamics and composition, and maintaining ecosystem health.

Therefore, the objective of this project is to aid decision makers with the capability of maintaining coastal ecosystem health (related to phytoplankton) by creating a prototype phytoplankton productivity information system over Galveston Bay. The developed prototype information system contains two parts: a monitoring component and a predicting component.

1) *Monitoring phytoplankton productivity through satellite remote sensing.* Since field measurements are complicated and expensive, satellite remote sensing provides an opportunity to observe real-time variations of Chlorophyll-*a* at a large spatial scale. In order to monitor the

variation of Chlorophyll-*a* with high accuracy, we developed algorithms using in-situ measurements, Landsat images, Moderate Resolution Imaging Spectroradiometer (MODIS) reflectance data, and Medium Resolution Imaging Spectrometer (MERIS) reflectance data.

2) *Predicting phytoplankton productivity using state-of-the-art modeling capabilities.* The prediction of phytoplankton productivity was conducted in three steps: (1) the Distributed Hydrology Soil Vegetation Model (DHSVM) was set up over the Trinity and San Jacinto River basins; (2) a long-term relationship between observed inflows and remotely sensed phytoplankton productivity was established; and (3) the model was then applied to conduct seasonal forecasting of phytoplankton driven by predicted seasonal weather forecasts from the National Centers for Environmental Prediction (NCEP) Climate Forecast System (CFS).

Specifically, the following six project tasks have been carried out:

1) Generating a high spatial resolution Landsat Chlorophyll-*a* concentration product**;**
2) Creating a long-term Chlorophyll-a concentration product from MODIS;
3) Calibrating and validating the Distributed Hydrology Soil Vegetation Model (DHSVM)
4) Identifying the relationship between inflows and phytoplankton productivity
5) Constructing and testing the phytoplankton productivity forecasting system
6) Implementing outreach activities to educate the public

In this project report, the study area—Galveston Bay and its upstream river basins— is described in Section 2. Each of the above tasks is addressed in one standalone section (i.e., Section 3 to Section 8). These sections are generally organized in the order of data, methods, and results.

2. Study Area

Galveston Bay (Figure 1)—also referred to as the Trinity-San Jacinto Estuary—is located along the upper coast of Texas and is connected to the Gulf of Mexico. It is the seventh largest estuary in the U.S., bordering the fourth largest city and fifth largest metropolitan area (by population) in the nation. Due to these factors and others, it is home to a substantial industrial and maritime center. There are two major watersheds providing inflow into this estuary: the Trinity Basin and the San Jacinto Basin. These basins are home to two of the largest cities in the U.S., Houston and Dallas, and include 60% of the major industrial facilities in Texas (Ornolfsdottir et al. 2004). Half of the population in Texas currently lives within those two watersheds.

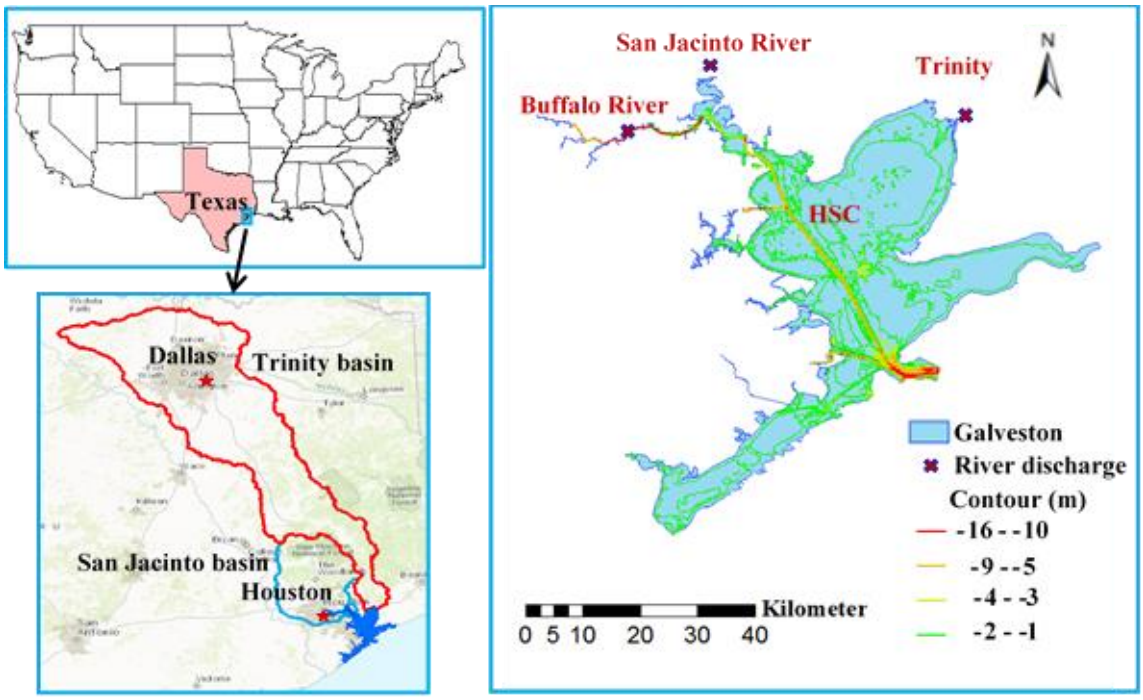

Figure 1. Galveston Bay and its upstream river basins.

Galveston Bay covers an area of 1360 km^2 and has an average depth of 2-3 m. There is a man-made channel—the Houston Shipping Channel (HSC)—with a depth of 15 m that extends

from the San Jacinto River in the northern part of the bay to the main Gulf entrance. Many lands surrounding Galveston Bay are highly urbanized and industrialized (especially Houston), which brings a significant amount of anthropogenic waste water into the bay. Armstrong and Ward (1993) reported that about 30 -60% of waste water in Texas is received by Galveston Bay. Freshwater inflows are primarily from two major rivers: the Trinity River and that San Jacinto River. Other smaller discharging rivers include Buffalo Bayou, Whiteoak Bayou, Brays Bayou, Huntingyon Bayou, Sims Bayou, and Greens Bayou. Historically, the San Jacinto River and the Trinity River contribute about 28% and 54% of total freshwater inflow, respectively (Roelke et al. 2013). According to U.S. Geological Survey (USGS) data from 2002 to 2012, the average discharge from the Trinity and the San Jacinto rivers are 211.2 m3/s and 67.7 m3/s respectively. In such a shallow bay, freshwater inflows are an important mechanism for water mixing. The nutrients loading input into Galveston Bay is very large, estimated to be 8.4 million kg/year of nitrogen and 4.0 million kg/year of phosphorus. However, the system has low to moderate Chlorophyll-a concentrations (2-20 μg/L), with an average concentration of 12.8 μg/L (based on field monitoring data from 2008 to 2015 provided by Dr. Antonietta Quigg).

In addition, Galveston Bay is located in a humid subtropical area of Texas, which is near the border of a semi-arid climate zone, making it much more vulnerable to extreme hydrological events and climate conditions (e.g. droughts and flood). The temperature range is roughly 4°C (winter) to ~ 32 °C (summer), and the annual rainfall is usually over 1000 mm. Heat from the deserts of Mexico and moisture from the Gulf of Mexico are brought into this area by prevailing winds from the south and southeast. At the same time, it is regularly impacted by tropical storms and hurricanes (especially during fall seasons). On September 12, 2008, Hurricane Ike arrived on

the south of Galveston, causing the whole coastal area of Galveston Bay to be inundated by saltwater.

3. Landsat based Chlorophyll-*a* product

3.1. Data and method

3.1.1. In-situ Chlorophyll-a measurements.

The *in-situ* observations used in this study were from 2009 to 2011, and the spatial distribution of the matchup points (with MERIS imagery) is shown in Figure 2. For this data, surface (0-0.3m) water samples were collected from 6 to 41 stations around Galveston Bay (number dependent on funded program sampling design). Samples were vacuum filtered (<130 kPa) onto 47mm Whatman GF/F filters and immediately frozen. Chlorophyll-a (corrected for pheophytin-*a*) was determined fluorometrically (Turner Designs 10-AU).

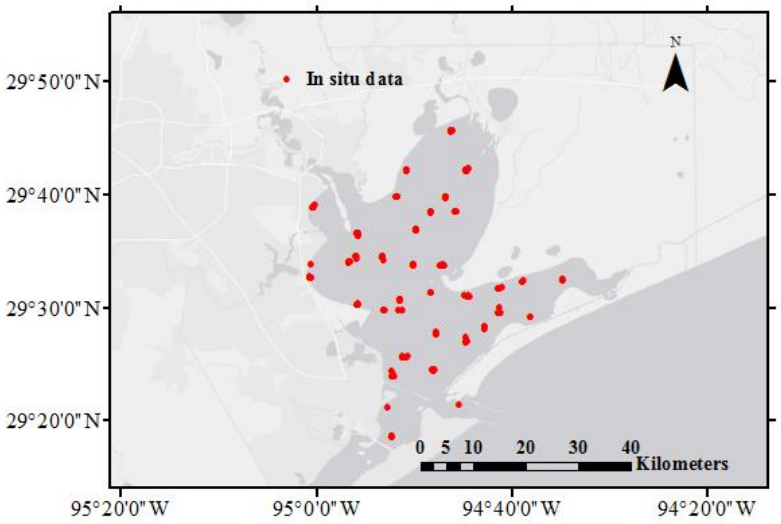

Figure 2. Locations of the in situ Chlorophyll-a sampling data.

3.1.2. Landsat Enhanced Thematic Mapper Plus (ETM+) data.

The Landsat 7 ETM+ surface reflectance product under the Universal Transverse Mercator (UTM) projection was ordered through the USGS at http://earthexplorer.usgs.gov/. Due to the Scan Line Corrector (SLC) failure, around 22 percent of any given Landsat-7 scene has been lost

since 2003. A linear interpolation approach was employed to fill in the missing data (due to the SLC failure) using the adjacent data on the same image. In order to match the geo-locations of the Landsat data with the in situ measured Chlorophyll-a precisely, the Galveston Bay area (29.75~ 29.35N, 95.35, 94.5W) was extracted and combined from two different Landsat scenes (i.e., 025 and 040), and then re-projected to the World Geodetic System (WGS) Latitude/Longitude. Then, a median smooth filtering operation with a size of 5 by 5 pixels was executed for each band to reduce the influences of Guassian noise.

Landsat based algorithm for estimating Chlorophyll-a. Based on the spectral features of Chlorophyll-a, a linear regression relationship was established between the gauge Chlorophyll-a concentration data and Landsat-7 band 4 reflectance data in the same geo-location at the same measurement time (Equation 1). Then this relationship was applied to all cloud-free Landsat images to develop the Chlorophyll-a concentration product.

$$y = 0.0161x + 7.293 \quad (1)$$

where x is the band 4 reflectance, and y is the Chlorophyll-a concentration.

3.2. Landsat based Chlorophyll-a results

The key information about the Landsat based Chlorophyll-a product is summarized in Table 1. Figure 3 shows a few selected images from the Landsat based Chlorophyll-a product. It suggests that the Chlorophyll-a concentrations tend to be higher during the spring than in the fall. Also, the Chlorophyll-a is higher on the east side of the bay than the west side during the spring. The concentration in the Houston Shipping Channel (HSC) area is clearly different from that in other regions. Although the Landsat-7 based Chlorophyll-a product has an advantage of high spatial resolution (30 m), it is strongly limited by the sensor's low return period (16 days) and its

sensitivity to cloud conditions. Therefore, the Landsat based product was not used for developing the relationship between river discharge and Chlorophyll-a.

Table 1. Landsat based Chlorophyll-a concentration product

Spatial resolution	30 m
Temporal resolution	16 days
Product period	2000 to 2011
Unit	µg/L

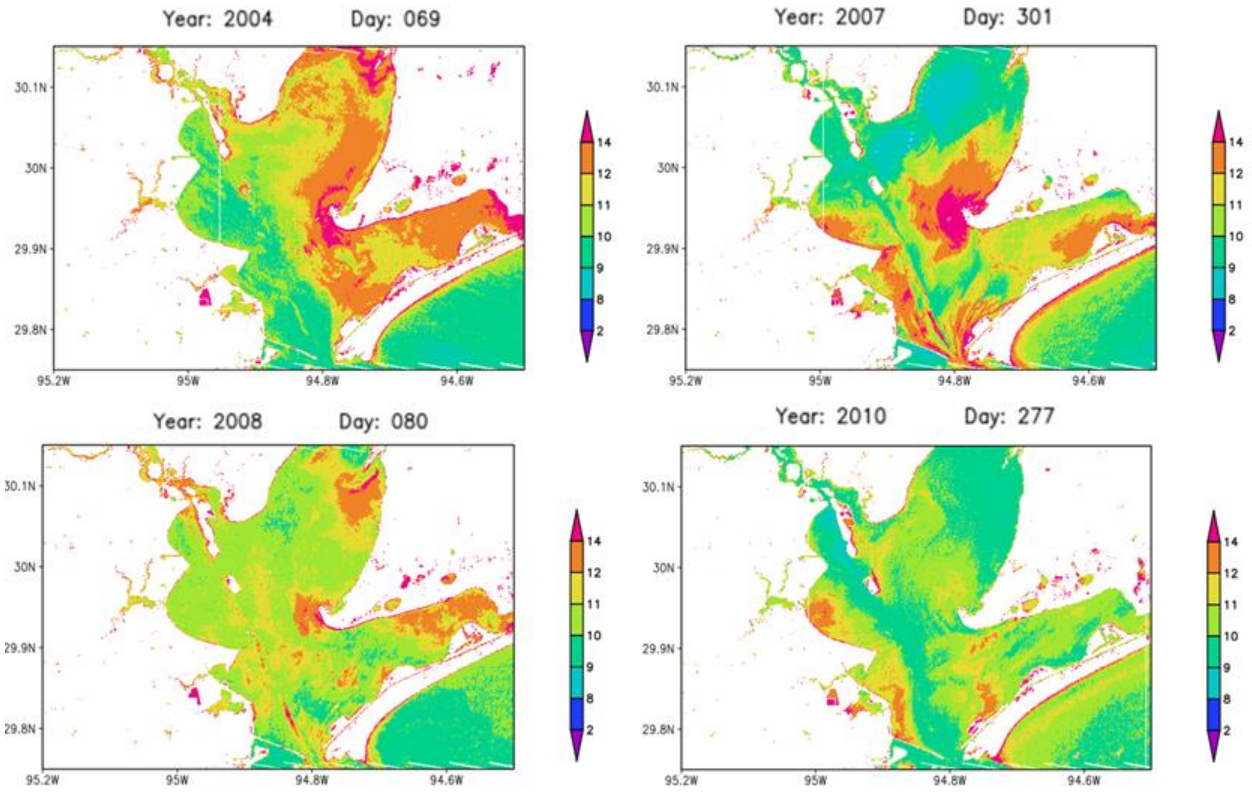

Figure 3. Selected results from the Landsat-7 based Chlorophyll-a concentrations.

4. MODIS and MERIS based Chlorophyll-*a* products

4.1. MODIS based product

4.1.1. MODIS data and method

MODIS Terra satellite Chlorophyll *a* estimations were created from 2000 to 2015 over the Galveston Bay area, using the surface reflectance products (MOD09Q1) which have an 8-day interval. The MDOSI product was calibrated against the Landsat-7 Chlorophyll-a product (see Section 3.2). The approach mainly contains two steps: MODIS data processing, and Chlorophyll-a concentration estimations.

(1) MODIS data processing

The MODIS 250m resolution reflectance images were first re-projected to WGS Latitude and Longitude. After the re-projection, the spatial resolution was 0.0025 degree. The Galveston Bay area (29.75~ 29.35N, 95.35~94.5W) was then extracted from each MODIS image of interest.

(2) Chlorophyll-a concentration retrieval

To reduce the effects of sensor measurement uncertainties on the Landsat-MODIS relationship, we compared the average values of the Landsat Chlorophyll-a images with the average of the MODIS based Chlorophyll-a reflectance ratio images over the period from 2000 to 2011. First, a total of 29 pairs of Landsat based Chlorophyll-a images and MODIS reflectance images were identified. Next, the Landsat Chlorophyll-a values (at 30 m resolution) were upscaled to 0.0025 degree resolution to match the MODIS reflectance. Then, the MODIS reflectance band ratio (R) between band 1 (b1) and band 2 (b2) was calculated as R = (b1+0.0101)/(b2+0.0101), where the offset value of 101 was introduced to avoid negative values. By pairing up the corresponding pixels from Landsat Chlorophyll-a with MODIS reflectance band ratio values within the bay area, a least square regression relationship was established (Equation 2). Last, the regression relationship was applied to each of the MODIS cloud-free reflectance images to derive the 8-day Chlorophyll-a product.

$$\text{Chlorophyll-a} = -5.96 \times R + 22.5 \quad (2)$$

4.1.2. MODIS based Chlorophyll-a results

A few selected images from the MODIS based Chlorophyll-a product are shown in Figure 4. Similar to the Landsat results, the MODIS 8-day product shows large spatial-temporal variations. Although the MODIS spatial resolution is much lower than that of Landsat, the temporal coverage has been improved significantly since the 8-day reflectance data were based on the composites of daily observations.

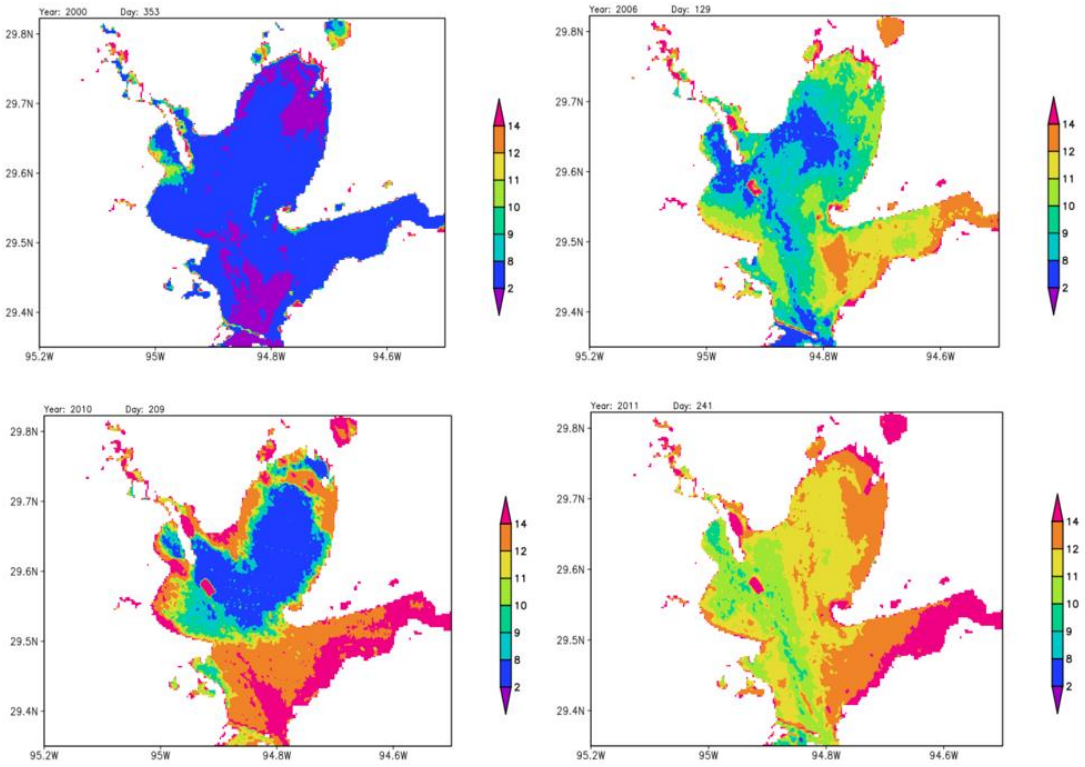

Figure 4. Selected results from the MODIS based Chlorophyll-a concentrations.

4.2. MERIS based product

Because MERIS bands are more sensitive to Chlorophyll-a than MODIS bands, we have developed a MERIS based algorithm (and product) for the period of 2002-2011 (the period when the sensor was functional) (Zhang et al., 2016). This product was used to identify the relationship between inflows and Chlorophyll-a concentrations discussed in Section 6.

4.2.1. MERIS data and method

MERIS is one of the main instruments carried by the Envisat satellite. Its spatial resolution is 260m by 300m (for land and coastal regions) with a repeat period of about 3 days. The MERIS Level 1b (L1b) band 7 (664 nm), band 8 (681 nm), and band 9 (708 nm) reflectance data were used in this study to calculate Fluorescence line height (FLH). FLH has an outstanding performance in retrieving Chlorophyll-a, and it has been applied in many studies. The auxiliary data (e. g. sun zenith angle, view zenith angle, view zenith angle, concentrations of ozone and water vapor) are utilized as the input data of the 6S model to carry out the atmospheric correction. One of the important input data sources for Satellite Signal in the Solar Spectrum model (6S model) is the aerosol optical depth (AOD). Here, AOD information was adopted from the MODIS level 3 Atmosphere 8-Day Global Product (MOD08_E3) at 1-degree resolution.

The retrieval of Chlorophyll-a from MERIS data involves four major steps, as shown in Figure 5. First, the pre-process of MERIS FR 1b data (e.g. the image subset and the SMILE effect correction—an artifact of the sensor type), is required. Second, the geometric biases of MERIS images were corrected against a reference image. Third, the 6S model was applied for atmospheric correction. The 6S model is designed to simulate the reflection of solar radiation by taking a wide range of atmospheric, spectral, and geometrical conditions into account. Last, a regressed linear relationship between the MERIS FLH values and in situ Chlorophyll-a measurements was established and applied to the MERIS FLH from each image during the study period. For this purpose, the MERIS FLH was calculated from the reflectance data using Equation 3.

$$FLH=b8 -C\times[b7+(b9-b7)(\lambda 8-\lambda 7)/ (\lambda 9-\lambda 7)] \quad (3)$$

where b7, b8, and b9 are the reflectance of bands 7, 8, and 9 from MERIS. C is a constant coefficient, which was set to 1.005 here. $\lambda 7$, $\lambda 8$, and $\lambda 9$ are the wavelengths of each band,

respectively. In establishing and testing the linear regression relationship, all of the pairs of MERIS FLH and the *in-situ* measured Chlorophyll-a concentrations were randomly divided into a training group and a validation group. The training group contains 70% of the total points which were used for the linear regression. The remaining 30% of the points were used to evaluate the performance of the algorithm. A regression relationship was then established in Equation 4:

$$y = 0.6344x + 4.917 \quad (4)$$

where y is the Chlorophyll-a and x is the FLH index.

The regression relationship (Equation 4) was then applied to each MERIS image from 2002 to 2011 to derive a ten-year Chlorophyll-a concentration product. For better extracting the temporal and spatial pattern of the concentration variations, the datasets were smoothed using the monthly running mean.

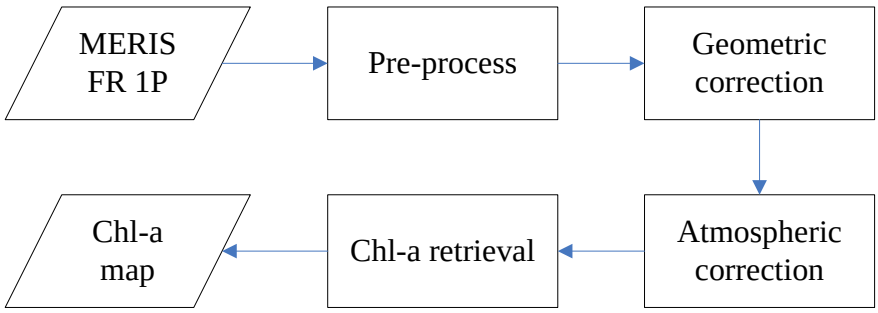

Figure 5. Flow chart of the MERIS based Chlorophyll-a retrieval algorithm

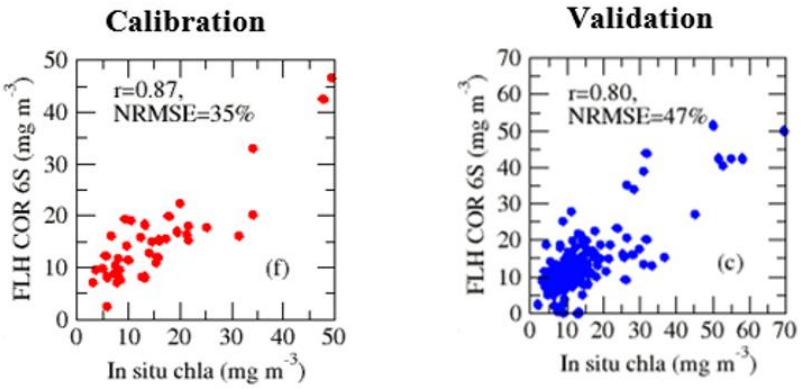

Figure 6. Calibration and validation results of the MERIS based Chlorophyll-a algorithm.

4.2.2. MERIS based Chlorophyll-a results

The MERIS based Chlorophyll-a results are summarized in terms of annual means, monthly climatology, and the associated standard deviations. Figure 7 suggests a strong inter-annual variability of Chlorophyll-a in Galveston Bay. Overall, the highest Chlorophyll-a concentration appears in 2010 (a wet year), then followed by a sharp decrease in 2011 (a drought year). Similar to the results concerning inter-annual variability, Figure 8 shows the distribution patterns of the monthly climatology. Chlorophyll-a concentration observably fluctuates, with the highest values occurring from February to May. For most of the time during the year, the high values tend to cluster around the northern segments (except for February when the largest Chlorophyll-a concentration occurs in the center of the bay). Higher monthly mean Chlorophyll-a concentrations are also accompanied by higher seasonal standard deviations. For instance, the Chlorophyll-a concentrations are relatively high across the whole bay in February, and the standard deviations of Chlorophyll-a in February are also found to be the highest among all of the months. In addition, from August to the following January, the spatial distribution of Chlorophyll-a is more homogeneous as compared with the other months (especially from February to May).

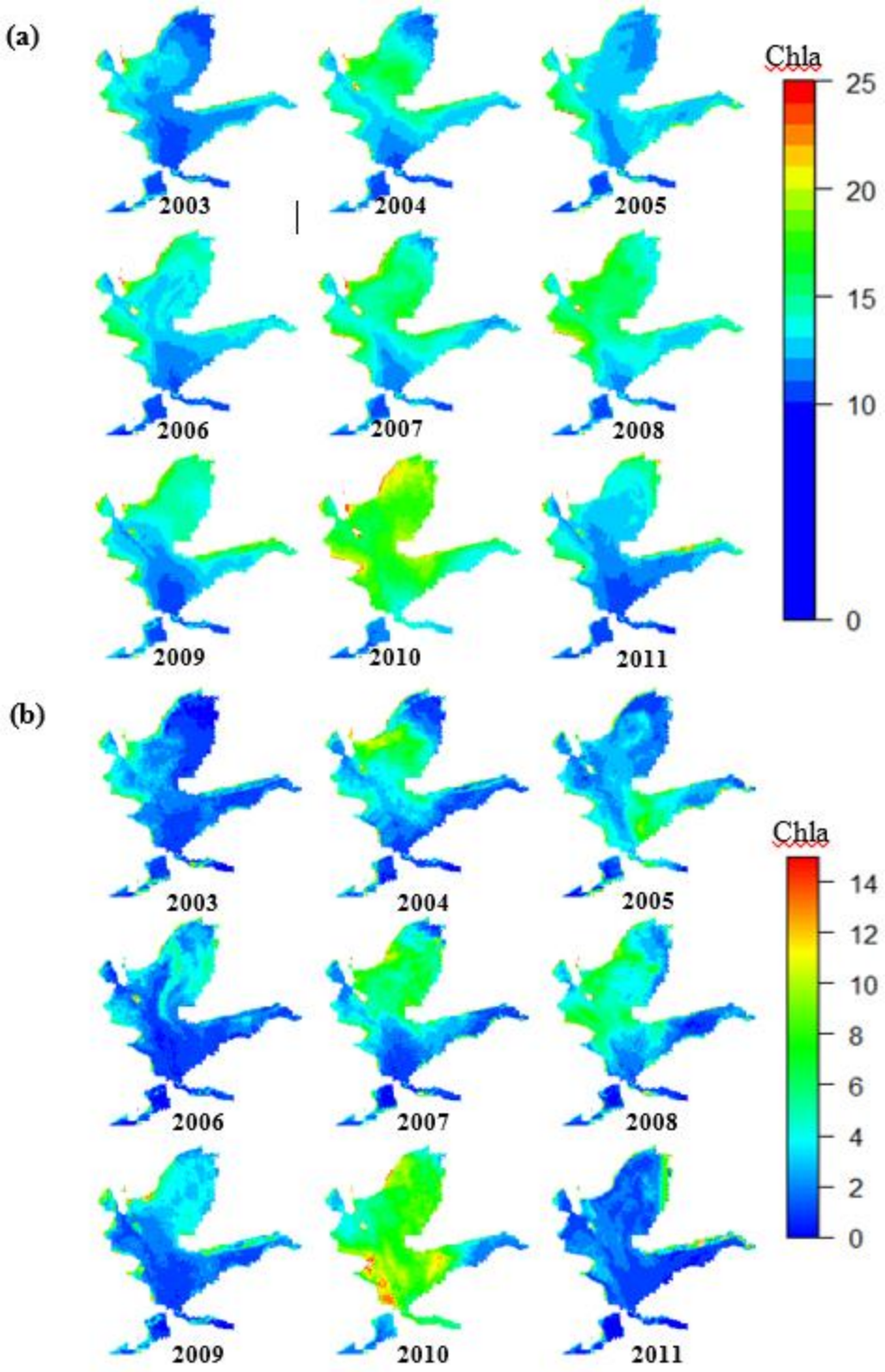

Figure 7. Annual Chlorophyll-a spatial distributions. (a) Mean Chlorophyll-a concentrations by year; (b) Standard deviation of Chlorophyll-a concentrations by year. Units: μg/L (2002 is excluded because of data limitations).

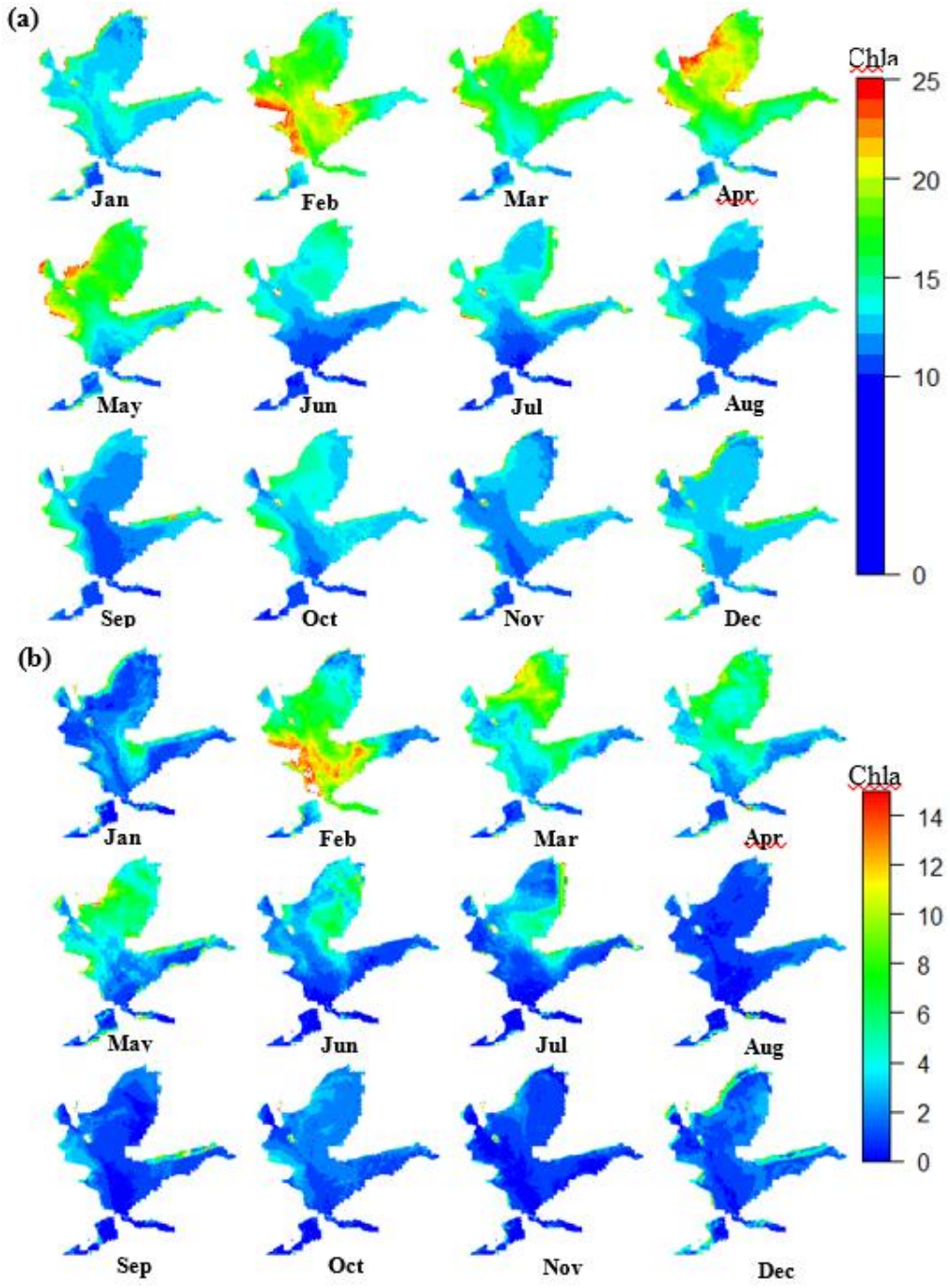

Figure 8. Monthly Chlorophyll-a spatial distributions. (a) Mean Chlorophyll-a concentrations by month; (b) Standard deviation of Chlorophyll-a concentrations by month. Unit: μg/L

5. Calibration and validation of the Distributed Hydrology Soil Vegetation Model (DHSVM)

5.1. The Trinity River Basin and the San Jacinto River Basin

The study sites for this section are the San Jacinto River Basin (SJRB; Figure 9) and Trinity River Basin (TRB; Figure 10), which are the major sources of inflows into Galveston Bay. The SJRB has a drainage area of 10,500 km^2, and the TRB has a drainage area of 44,900 km^2. According to the United States Geological Survey (USGS) hydrologic unit code classifications, the SJRB is divided into four subbasins: the East Fork San Jacinto, West Fork San Jacinto, Cypress Creek, and White-oak Bayou watersheds. Specifically, most of the Houston metropolitan area is located in the White-oak Bayou watershed. The TRB is divided into seven subbasins: the Elm Fork Trinity, East Fork Trinity, West Fork Trinity, Cedar and Upper Trinity, RiChlorophyll-and, Lower Trinity-Tehuacana, and Lower Trinity-Kickapoo watersheds. The Dallas-Fort Worth metropolitan area is mainly located in the upstream subbasins (Elm Fork Trinity, East Fork Trinity, and West Fork Trinity).

Because of the high frequency of heavy rainfall events in the SJRB, river floods have been a serious issue for the local residents. In addition, the rapid urban expansion of Houston has caused additional concerns about larger potential flood damages under the context of climate change. In order to reduce the flood risk in the city area, the U.S. Army Corps of Engineers constructed two flood control reservoirs upstream of the White-oak Bayou—the Addicks and Barker reservoirs. Both reservoirs are used both as recreational parks and as flood control reservoirs. Since the construction of these dams, flood damages in the city of Houston have been significantly reduced. The annual average damage reduction is estimated to be about 16 million dollars.

On the other hand, policy makers in the TRB are more concerned about droughts than floods. Delivering water to both Dallas and Houston, the Trinity River plays an important role in the regional water supply system. There are 16 reservoirs in the TRB that have a capacity of more than 40 million m^3. The combined conservation storage of these reservoirs is about 9 billion m^3. However, under the impacts of climate change, it remains a critical issue to assess if these reservoirs are sufficient to provide reliable and sustainable water supply to the two megacities.

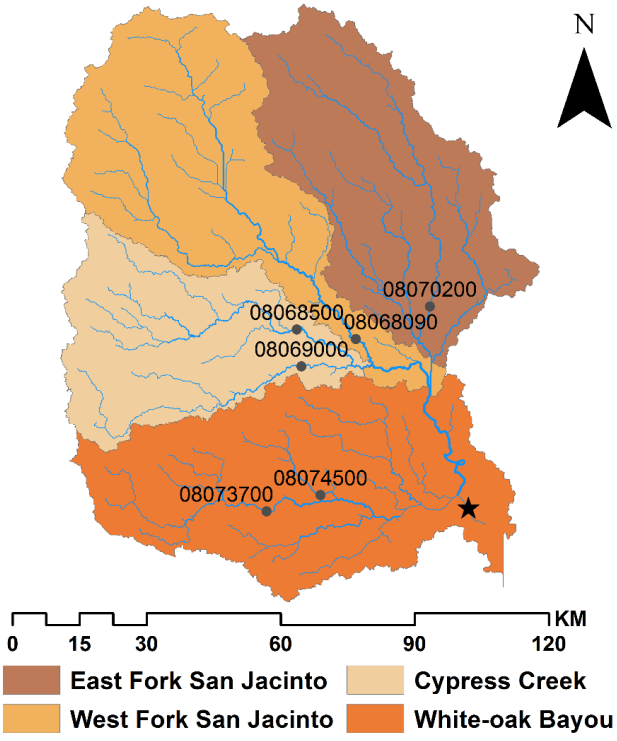

Figure 9. The San Jacinto River Basin including its 4 subbasins. Black points represent USGS streamflow monitoring gauges.

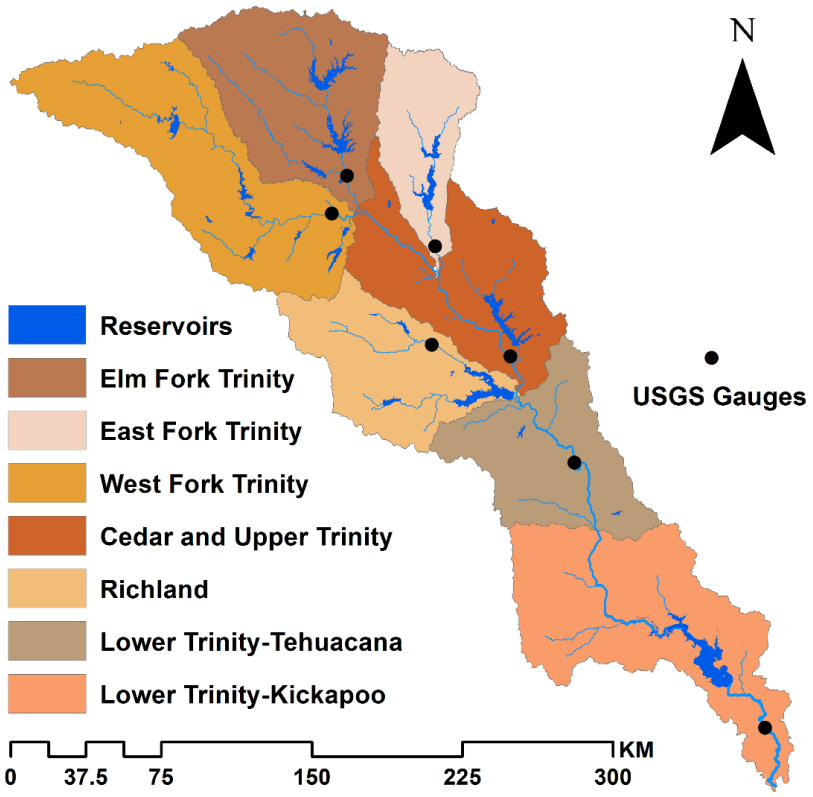

Figure 10. The Trinity River Basin including its 7 subbasins. Black points represent USGS streamflow monitoring gauges, and blue areas represent reservoirs.

5.2. The DHSVM model and input data

The Distributed Hydrology Soil Vegetation Model (DHSVM, Wigmosta et al., 1994) was employed in this project to simulate the inflows into Galveston Bay. DHSVM explicitly simulates the water and energy balance across the domain at a high spatial resolution (e.g. 10 m to 200 m). The model is physically based and can represent hydrological processes such as evapotranspiration, infiltration, snowmelt, and urban area detention. It calculates evapotranspiration using a full energy balance method, and also accounts for the evaporation from the canopy intercepted water. Overland, surface and subsurface runoff (including unsaturated and saturated) water for each grid cell is routed to its downslope neighbor cells (based on topography) until the water reaches the stream channels. Within the stream, the

simplified Muskingum-Cunge routing method is used for each river segment at each time step. DHSVM can simulate streamflow at a sub-daily time step over multiple years. Because of the hyper-resolution that this model is built upon, it can adequately represent the heterogeneity of the target site. Specifically, the fact that urban impervious coverage can be explicitly simulated in DHSVM makes it suitable to be used in both the SJRB and the TRB. In addition, when accommodated with the newly added reservoir module, DHSVM can also simulate the hydrologic effects of multiple reservoirs (Zhao et al, 2016).

Input data for DHSVM include a digital elevation model (DEM), a land use land cover (LULC) map, a soil texture map, stream network information, and meteorological data. The DEM was downloaded from the Shuttle Radar Topography Mission Digital Elevation Database, LULC was obtained from the National Land Cover Database (NLCD) 2006, and the Soil Texture map was obtained from the Soil Survey Geographic Database (SSURGO). With respect to the meteorological data, we used the products developed by Livneh et al. (2013). To take advantage of the hyper-resolution modelling framework of DHSVM, we used 90m spatial resolution for the SJRB and 200m for the TRB (considering the size of each basin)—and then we resampled the LULC and soil texture maps to these same resolutions. For both river basins, the temporal resolution we used in this study was 3-hourly.

The DHSVM input data include spatially static and temporally varied data. Temporally varied meteorological forcing data include precipitation, temperature, relative humidity, incoming longwave/shortwave radiation, and wind speed. Spatially static data include a digital elevation map (DEM), a basin boundary mask, soil depth, soil texture, land cover types, channel distribution, and morphology information. In this study, the DEM was obtained from the Shuttle Radar Topography Mission (SRTM) 30 m resolution product, which was then resampled to 200

m (i.e. the DHSVM grid cell resolution). Based on the DEM information and the hydrometric station locations, Geographical Information System (GIS) tools were used to generate the soil depth map, the river network, and the basin boundary mask. The soil texture was acquired from the State Soil Geographic (STATSGO) Database (Miller and White, 1998).

5.3. Calibration and validation results

There are multiple streamflow monitoring stations inside of the SJRB and the TRB. In this study, we chose six gauges in the SJRB and seven in the TRB to calibrate and validate the DHSVM. The selection of these gauges was based on the location of the subbasins—aiming to select at least one gauge for each subbasin. In addition, all selected gauges have consecutive monitoring records that cover the calibration period. In order to capture the streamflow variability on a fine time scale in the SJRB, we used weekly streamflow data to calibrate and validate DHSVM. With respect to the TRB, considering the large size and the associated computational expense, we used a monthly time step to represent the seasonality.

As a physically based hyper-resolution model, DHSVM has three sets of parameters which include soil parameters, vegetation parameters, and other calibrated parameters. Based on a parameter sensitivity test, we adjusted: the 4 soil parameters (porosity, wilting point, vertical conductivity, and maximum infiltration), and the 3 vegetation parameters (monthly leaf area index (LAI), canopy resistance, and vapor pressure deficit). The calibrated streamflow for the SJRB can be found in Figure 11, and the corresponding error statistics are shown in Table 2 (which also contains the error statistics of the validation period). The TRB calibration and validation results can be found in Figure 12 and Table 3.

For both river basins, the PBIAS, the coefficient of determination (R^2), and the Nash–Sutcliffe efficiency (NSE) values show good agreement between observed and simulated

streamflow and reservoir storage. The NSE values of streamflow range from 0.58 to 0.88 for the calibration period, and from 0.56 to 0.83 for the validation period. With respect to the reservoir storage simulations, the Addicks and Barker reservoirs show reasonable agreement (with NSE values ranging from 0.66 to 0.80). The combined reservoir storage for the TRB has a NSE value of 0.84 for the calibration period and a value of 0.96 for the validation period, indicating a promising level of water viability evaluation using this modelling framework.

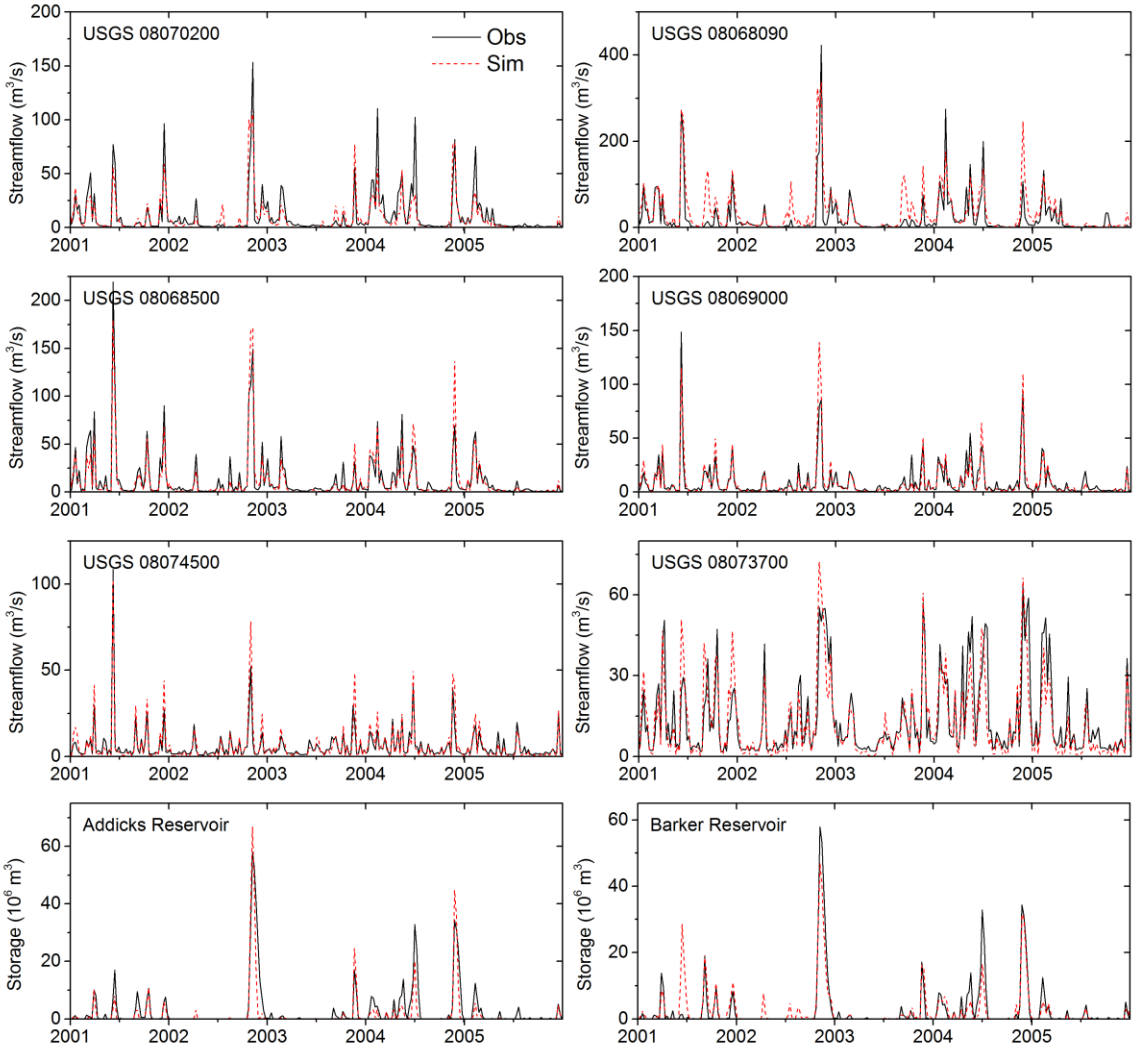

Figure 11. Streamflow and reservoir storage calibration results of DHSVM in the SJRB from Jan 1, 2001 to Dec 31, 2005.

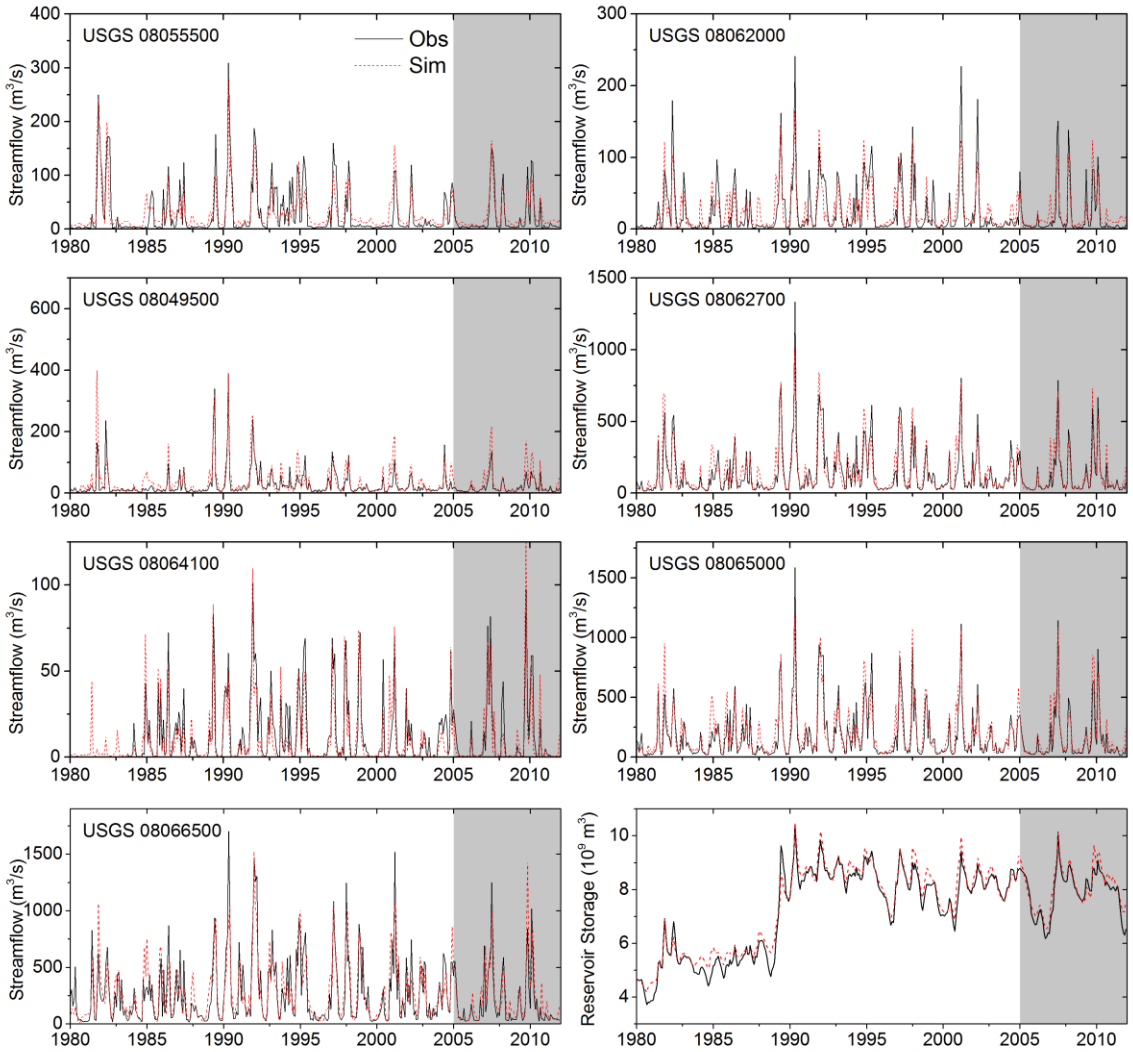

Figure 12. Streamflow and reservoir storage calibration and validation results of DHSVM in the TRB from Jan 1, 1980 to Dec 31, 2011. Reservoir storage in the last panel represents the combined storage for all of the 16 reservoirs in the TRB.

Table 2. Weekly error statistics of DHSVM performance for calibration and validation in the SJRB.

USGS gauge	Calibration (2001-2005)			Validation (1980-2000)		
	PBIAS	R^2	NSE	PBIAS	R^2	NSE
08070200	-20.3%	0.76	0.73	-19.5%	0.83	0.78
08068090	-2.8%	0.71	0.58	27.9%	0.64	0.61
08068500	-7.2%	0.87	0.86	-2.8%	0.71	0.67
08069000	-1.0%	0.84	0.81	9.2%	0.76	0.75
08074500	3.2%	0.91	0.84	13.1%	0.84	0.63
08073700	-8.5%	0.73	0.71	-7.5%	0.61	0.56

Addicks	-15.0%	0.78	0.76	-13%	0.67	0.66
Barker	-2.6%	0.80	0.80	-5.1%	0.73	0.68

Table 3. Monthly error statistics of DHSVM performance for calibration and validation in the TRB.

USGS gauge	Calibration (2005-2011)			Validation (1980-2004)		
	PBIAS	R^2	NSE	PBIAS	R^2	NSE
08055500	23.4%	0.90	0.87	4.0%	0.77	0.76
08062000	18.3%	0.83	0.81	5.0%	0.68	0.68
08049500	22.6%	0.88	0.61	19.0%	0.73	0.62
08062700	10.0%	0.89	0.87	6.8%	0.83	0.83
08064100	-5.0%	0.80	0.78	-26.3%	0.81	0.78
08065000	18.4%	0.90	0.88	12.7%	0.83	0.82
08066500	18.1%	0.65	0.58	5.3%	0.67	0.66
Storage	2.6%	0.90	0.84	2.5%	0.97	0.96

6. Relationship between inflows and phytoplankton productivity

6.1. Segmentation of the Galveston Bay

To better represent the influence of freshwater inflow, Galveston Bay was divided into five sub-regions based on Chlorophyll-a distribution and hydrodynamic conditions, as simulated by the Environmental Fluid Dynamics Code (EFDC) during the period of January 1st, 2005 to December 31th, 2006 (Shen et al. 2016). These sub-regions are Trinity Bay, San Jacinto Bay, East Bay, Lower Bay, and West Bay (Figure 13). This study explores the key factors driving Chlorophyll-a, and constructs a prediction model using these factors in each of the five sub-bays.

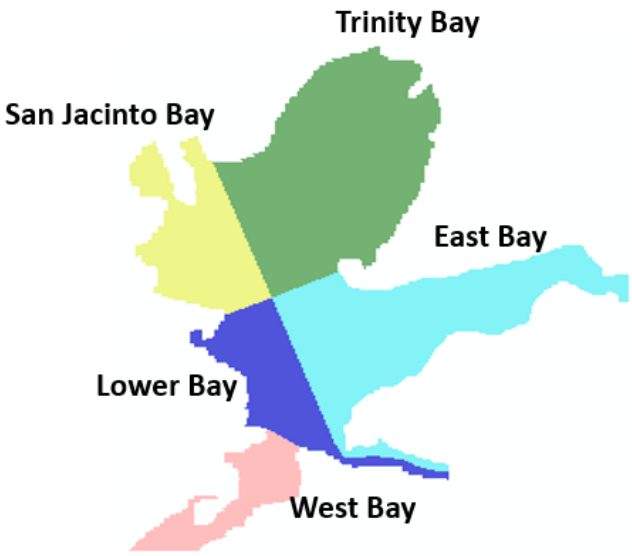

Figure 13. The Five Sub-Bays that comprise Galveston Bay

6.2. Data and method

6.2.1. Data

The datasets used for constructing the Chlorophyll-a multi-variable regression model are: the MERIS based Chlorophyll-a concentration in Galveston Bay, the observed discharge from both the Trinity and San Jacinto rivers, water temperature (from NOAA station # 8771013, Eagle Point, TX), and the Multivariate El Niño-Southern Oscillation Index (MEI). The period of data coverage is from May 22, 2002 to Dec 31, 2011 (roughly 10 years in total).

Four seasonal groups are defined, which are: (1) JFM - January, February and March; (2) AMJ - April, May and June; (3) JAS - July, August and September; (4) OND - October, November and December. For all four seasonal groups, Chlorophyll-a anomalies, freshwater inflow anomalies, and water temperature anomalies were calculated by subtracting their monthly climatological values (Equations 5-7).

$$C_{Chlorophyll\text{-}a} = C_{clim} + C_{anom} \quad (5)$$

$$C_{anom} = f_1 (Q_{anom}, T_{wanom,} MEI) \quad (6)$$

$$T_{water} = f_2 (T_{air}) \quad (7)$$

where $C_{Chlorophyll\text{-}a}$ is the Chlorophyll-a concentration, C_{clim} is the climatological average value of Chlorophyll-a, C_{anom} is the Chlorophyll-a anomaly, Q_{anom} is the river discharge anomaly, T_{wanom} is the water temperature anomaly, MEI is the Multiple ENSO Index value from NOAA, and T_{water} and T_{air} are the water and air temperature, respectively.

6.2.2 Identification of key driving factors of each segment

Although Chlorophyll-a concentrations are indispensable to river inflows (Figure 14), they could also be affected by other environmental factors such as water temperature and MEI (Figure 15).

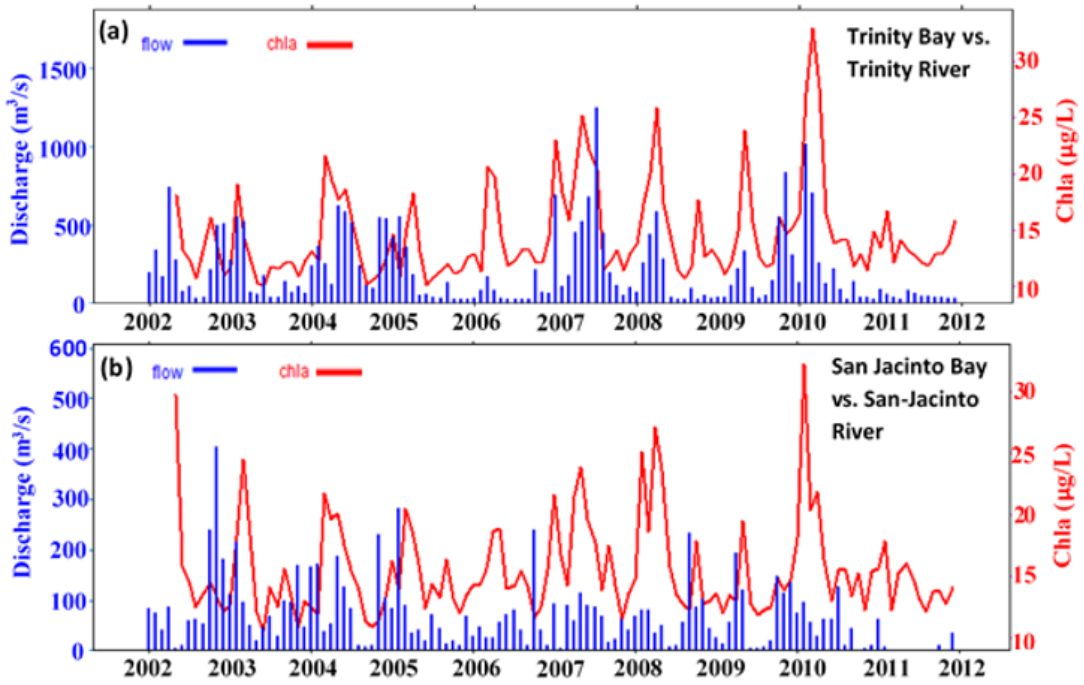

Figure 14. Time series of the monthly discharge and Chlorophyll-a concentration in (a) Trinity Bay and (b) San Jacinto Bay

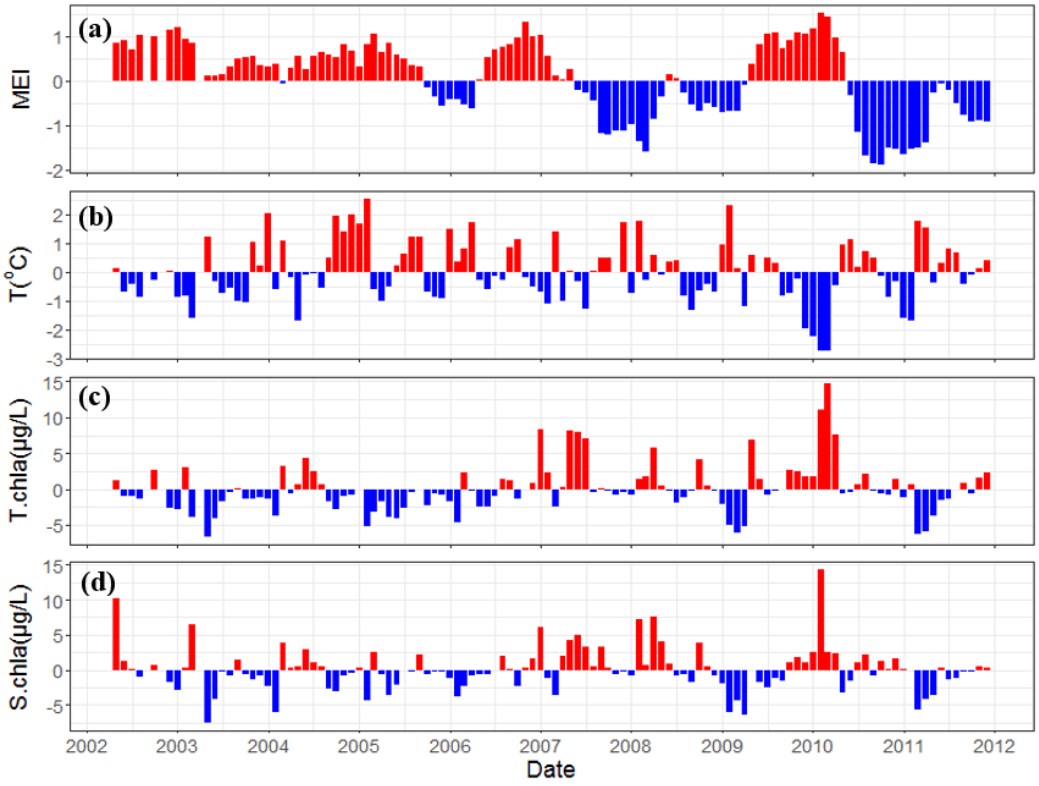

Figure 15. Time series of: (a) MEI (blue represents La Niña, and red is for El Niño); (b) water temperature anomalies; (c) Chlorophyll-a anomalies from Trinity Bay; (d) Chlorophyll-a anomalies from San Jacinto Bay.

The correlation coefficients between the Chlorophyll-a anomalies and the anomalies of the aforementioned environmental factors were then compared and ranked for each season, such that the most influential factors for each segment (subbay) could be identified. Figure 16 shows an example how the key environmental factors—which are significantly correlated with Chlorophyll-a anomalies—were found in Trinity Bay and San Jacinto Bay in the four seasonal groups. Table 4 summarizes all of the key factors identified through this process. It suggests that discharge is a key factor in the Trinity, San Jacinto, East, and Lower bays during most seasons. Trinity and San Jacinto Bay (which are close to the river outlets) are more affected by water temperature in OND and JFM, while the East and Lower bays are also affected by MEI during

JFM. West Bay is least affected by these factors, largely due to its various exchanges with the greater ocean.

(a)

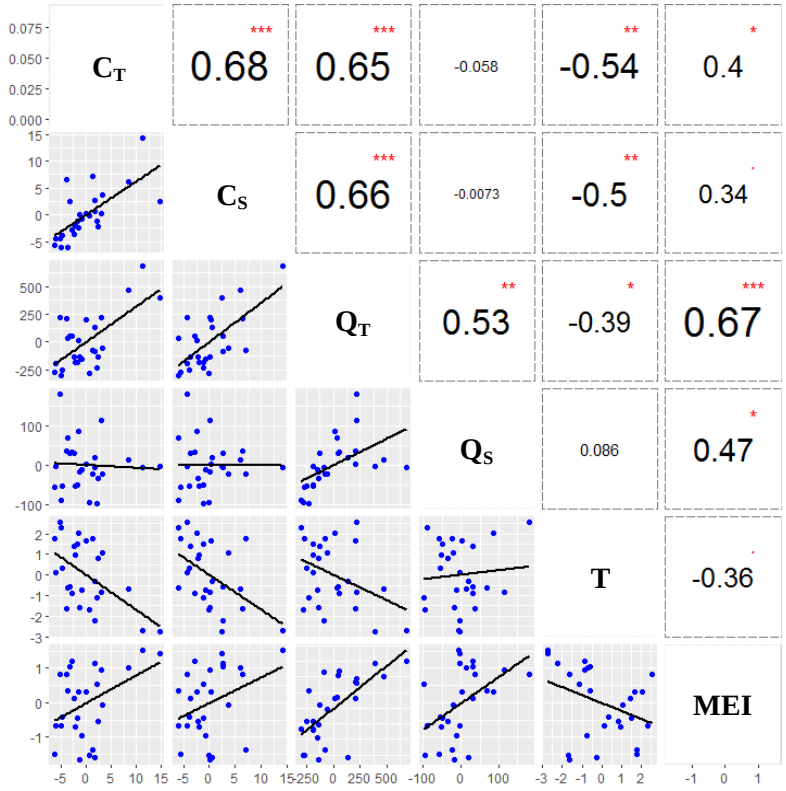

(b)

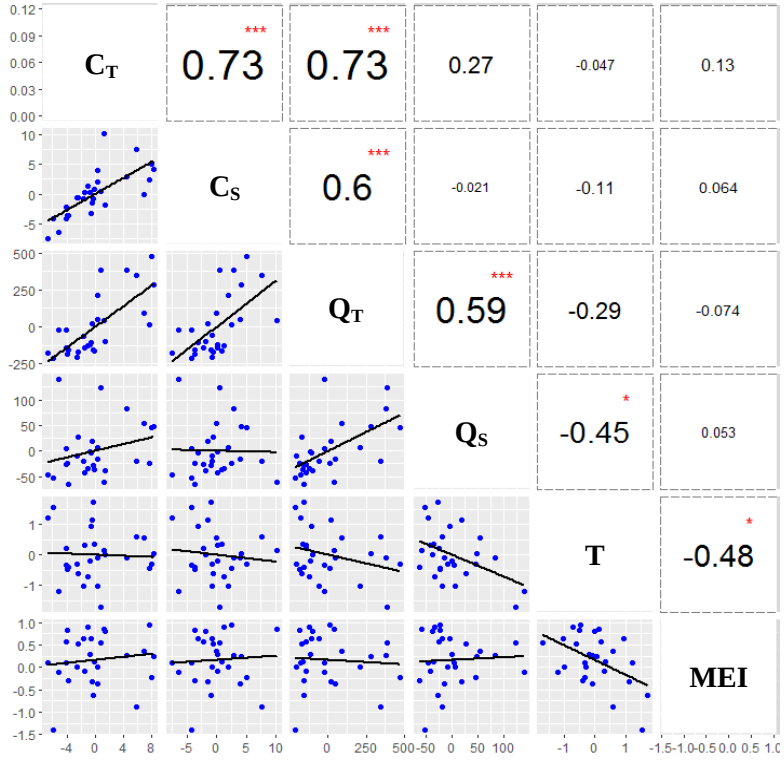

(c)

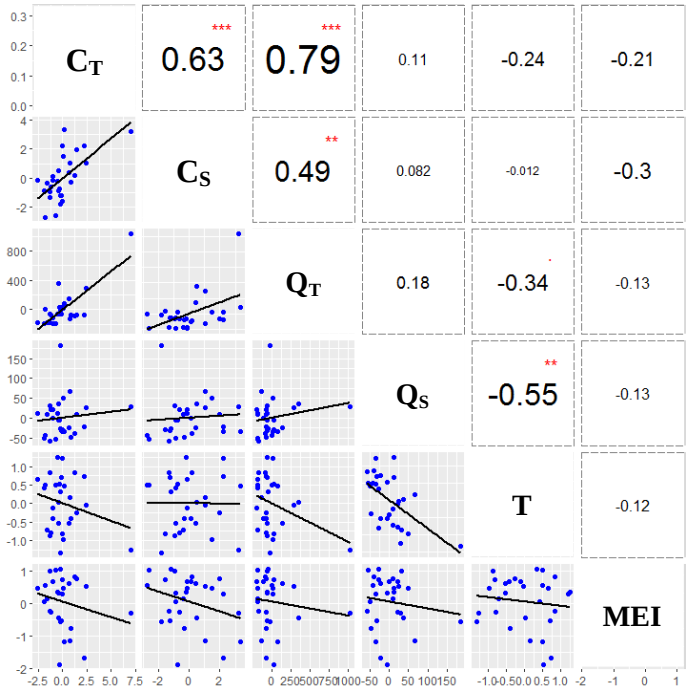

(d)

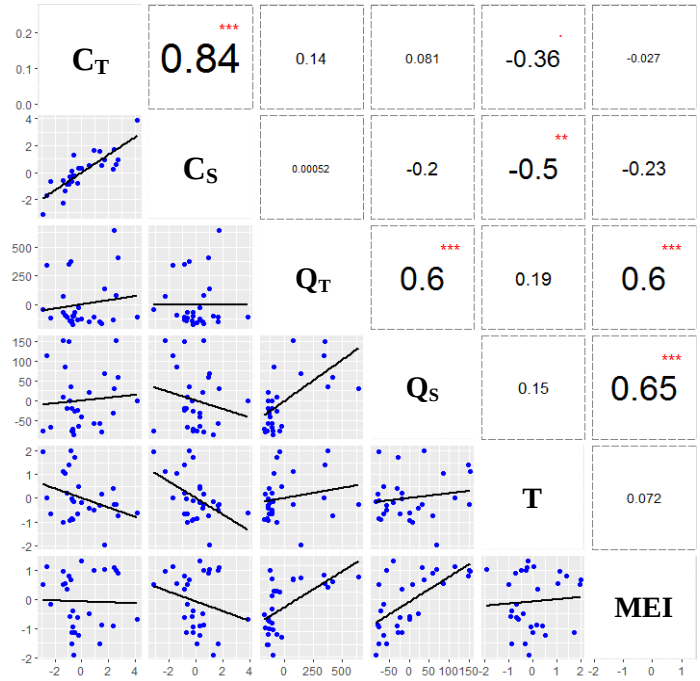

Significant codes: p < 0.001 *; 0.001< p < 0.01 **; 0.01 <p < 0.05 *; 0.01<p<0.1 .**

Figure 16. The monthly average correlation among C_T (Chlorophyll-a anomaly in the

Trinity Bay, µg/L), C_S (Chlorophyll-a anomaly in the San Jacinto Bay, µg/L), T (water temperature anomaly, °C), MEI (Multiple ENSO Index from NOAA), Q_T (discharge anomaly from the Trinity River, m^3/s) and Q_S (discharge anomaly from the San Jacinto River, m^3/s) in (a) JFM; (b) AMJ; (c) JAS and (d) OND.

Table 4. Key driving factors of Chlorophyll-a in each seasonal group (*p<0.01*)

Segments	Key driving factors of Chlorophyll-a (*p<0.01*)			
	JFM	**AMJ**	**JAS**	**OND**
Trinity Bay	Q & T	Q	Q	T
San Jacinto Bay	Q & T	Q	Q	T
East Bay	Q & MEI	Q	Q	Q
Lower Bay	Q & MEI	Q	Q	T *
West Bay	Q & MEI	MEI *	NA	NA

* *p<0.05*

6.3.Chlorophyll-a multi-variable regression model and model performance

6.3.1 Trinity Bay and San Jacinto Bay

Because Trinity Bay and San Jacinto Bay are both affected by the same key driving factors, one set of prediction models was developed by combining the two bays.

Table 5. Prediction models developed for the Trinity and San Jacinto Bay combined.

Seasonal group	equation	R^2	MAE	RMSE	p-value
JFM	$C_{avg} = 0.107 + 0.014\ Q_T - 0.040 Q_S$	0.64	1.75	2.03	<0.01**
AMJ	$C_{avg} = -0.084 + 0.013 Q_T$	0.73	1.97	2.33	<0.001***
JAS	$C_{avg} = -0.134 + 0.005 Q_T$	0.75	0.71	0.95	<0.001***
OND	$C_{avg} = -0.351 - 0.580 T$	0.29	1.09	1.40	0.10·

Significant codes: p < 0.001 *; 0.001< p < 0.01 **; 0.01 <p < 0.05 *; 0.01<p<0.1·**

Where C_{avg} is the Chlorophyll-a anomaly of the entire upper segment (Trinity and San Jacinto); Q_T is the discharge anomaly for the Trinity River; Q_S is the discharge anomaly for the San Jacinto River; and T is the water temperature anomaly.

By adding the climatology to the anomalies after Equations 5-7, the time series of Chlorophyll-a over the combined segments can be estimated (Figure 17).

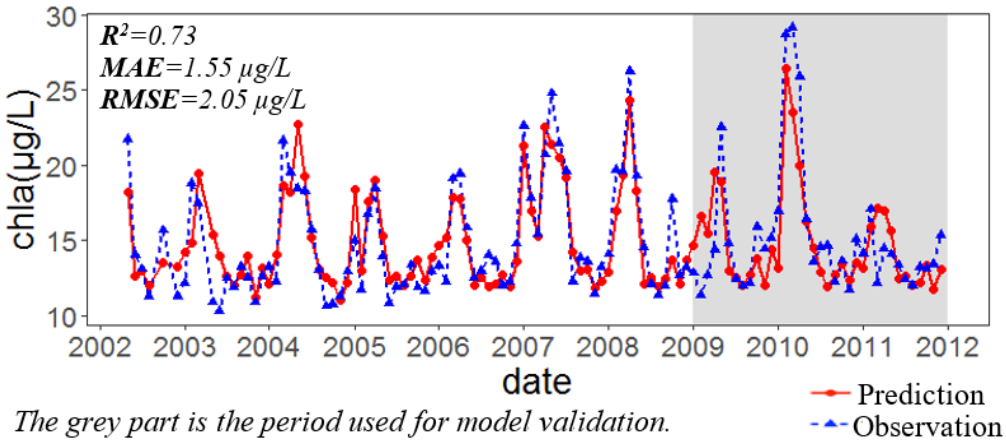

Figure 17. Model simulation and prediction results for Trinity and San Jacinto Bays combined (the shading indicates the testing period)

6.3.2 East Bay and Lower Bay

The prediction models for East Bay and Lower Bay are provided in Table 6, and the corresponding Chlorophyll-a estimations are shown in Figure 18.

Table 6. Prediction models developed for (a) East Bay; (b) Lower Bay.

(a)

Seasonal group	equation	R^2	MAE (µg/L)	RMSE (µg/L)	p-value
JFM	$C_E = -0.728 + 0.010Q_T$	0.39	1.91	2.31	<0.01**
AMJ	$C_E = -0.037 + 0.006Q_T$	0.78	1.01	1.22	<0.001***
JAS	$C_E = -0.105 + 0.004Q_T$	0.50	0.80	0.98	<0.001***
OND	$C_E = -0.662 - 0.001\ Q_T$	0.22	0.81	1.01	0.46

(b)

Seasonal group	equation	R^2	MAE (µg/L)	RMSE (µg/L)	p-value
JFM	$C_L = -0.869 + 0.013Q_T$	0.34	2.44	3.00	<0.01**
AMJ	$C_L = -0.318 + 0.007Q_T$	0.68	1.34	1.55	<0.001***
JAS	$C_L = -0.029 + 0.002Q_T$	0.46	0.56	0.74	<0.01**
OND	$C_L = -0.080 - 0.356T$	0.24	2.13	2.68	0.25

Significant codes: p < 0.001 *; 0.001< p < 0.01 **; 0.01 <p < 0.05 *; 0.01<p<0.1 .**

Where C_E is the chla anomaly of East Bay, and C_L is the chla anomaly of Lower Bay.

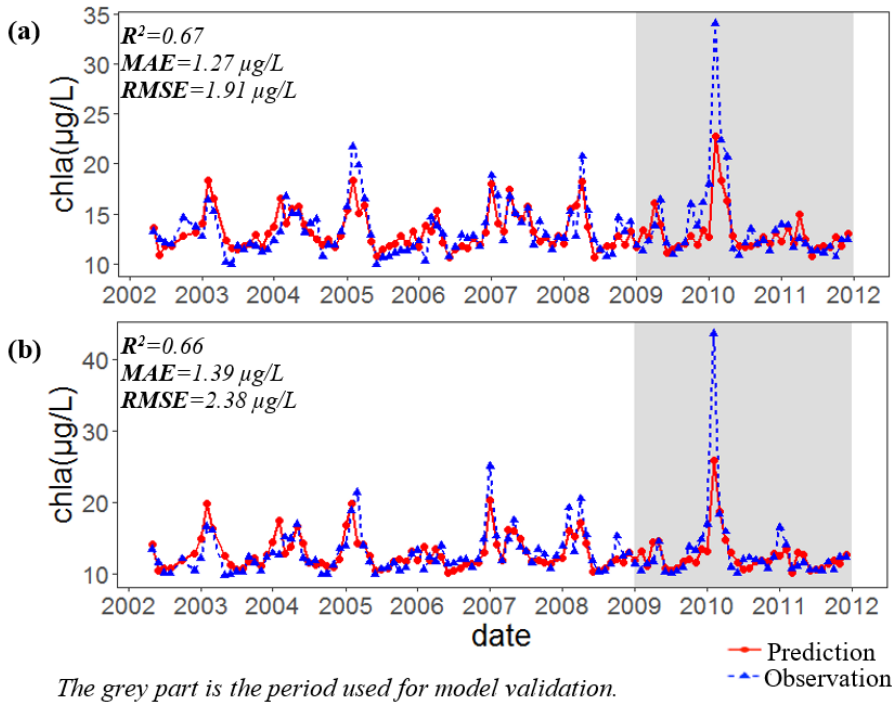

Figure 18. Model simulation and prediction results for a) East Bay and b) Lower Bay (the shading indicates the testing period).

6.3.3. West Bay

The prediction models for West Bay are provided in Table 7, and the corresponding Chla estimations are shown in Figure 19.

Table 7. Prediction models developed for West Bay

Seasonal group	equation	R^2	MAE (µg/L)	RMSE (µg/L)	p-value
JFM	C_W = -0.132 + 1.156MEI	0.57	0.94	1.18	<0.01**
AMJ	C_W = -0.166 + 0.259MEI	0.13	0.70	0.92	0.59
JAS	C_W = 0.0004	0.04	0.47	0.68	
OND	C_W = 0.0008	0.65	0.79	1.13	

Significant codes: p < 0.001 *; 0.001< p < 0.01 **; 0.01 <p < 0.05 *; 0.01<p<0.1·**
Where C_w is the Chlorophyll-a anomaly of West Bay

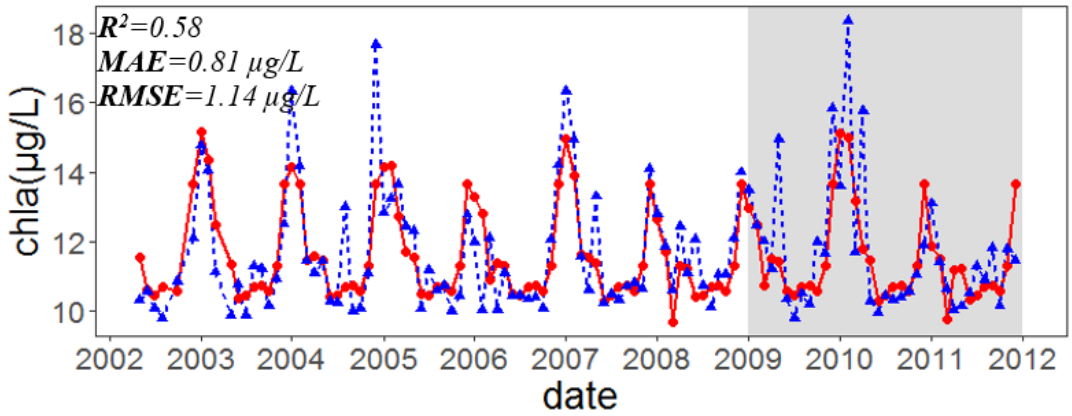

Figure 19. Model simulation and prediction results for West Bay (the shading indicates the testing period).

7. Chlorophyll-a forecasting system

7.1. Seasonal forecast of river inflows and water temperature

To forecast Chlorophyll-a concentrations, the river inflows and water temperatures needed to be predicted. To achieve this, seasonal climate forecast data were first downloaded from the North American Multi-Model Ensemble (NMME) system (http://www.cpc.ncep.noaa.gov/products/NMME/). Each model in the NMME system provides a climate forecast for the 12 months following the present month (for example, in August 2017 NMME models provide the climate forecast from September 2017 to August 2018). However, for quality control purposes, the current version of NMME only provides monthly forecasted

data for recent months. The most up-to-date forecasted daily data (including precipitation and air temperature) are only available for the years before 2012. Because hydrological forecasting needs daily climate input data, we used the most recently available daily data to demonstrate how forecast climate information can be used as inputs into the prediction model to estimate the Chlorophyll-a concentration in Galveston Bay (Section 6).

The forecasted daily data from January 2011 to December 2011 were downloaded from five climate models: CanCM3, CanCM4, CCSM4, GEOS-5, and GFDL. The meteorological forecasts from the first four models are at a spatial resolution of 1 degree, while the GFDL model outputs are at 0.625 degree. The climate model outputs include Precipitation, Max Temperature, and Min Temperature—which were subsequently used to drive the DHSVM model. For the Trinity River Basin, the DHSVM model was set up at a 200-meter spatial resolution and a 3-hourly time step. For the San Jacinto River Basin, DHSVM was set up at a 90-meter spatial resolution because the topography for this basin is relatively flat and because the basin size is small. The calibration and validation of DHSVM has been described in the deliverables for Task 3. The DHSVM was driven by the NMME seasonal forecast to simulate the Trinity River discharge (Figure 20). The discharge and water temperature were further used to predict the

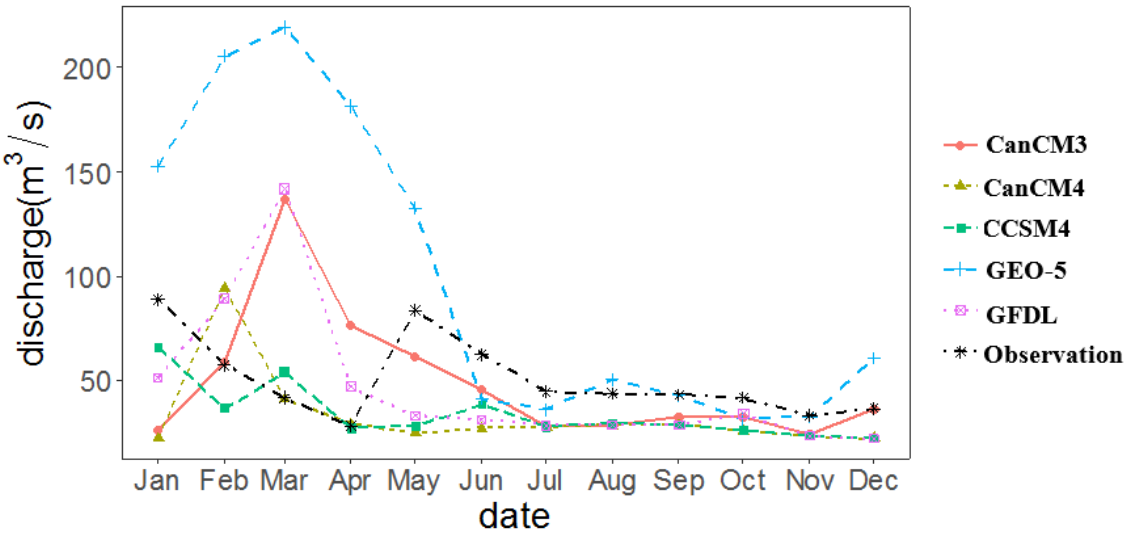

Figure 20. DHSVM simulated Trinity River discharge driven by NMME seasonal forecasts.

Chlorophyll-a concentration in Galveston Bay.

Because the water temperature is difficult to model, we used an empirical regression method to estimate the water temperature from the climate model forecasted air temperature. The linear relationship between the air and water temperature was developed using observation data (Figure 21). Hourly water temperature data were acquired from the Texas Water Development Board (TWDB). Because there are no significant differences among water

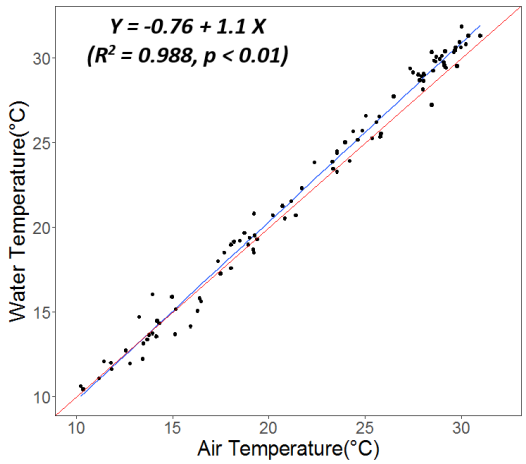

Figure 21. Linear regression relationship between observed air temperature and observed water temperature.

temperature values over different locations, the site located at the Boli monitoring station (latitude# 29.66°, longitude# -94.75°) was selected for the analysis. Hourly air temperature data were also collected by NOAA (Station# WBAN 12923, GALVESTON SCHOLES FIELD TX US). In both cases, observations were averaged to monthly values to develop the relationship shown in Figure 21. By applying this relationship to the climate model simulated monthly air temperatures, the corresponding water temperatures can be calculated (Figure 22).

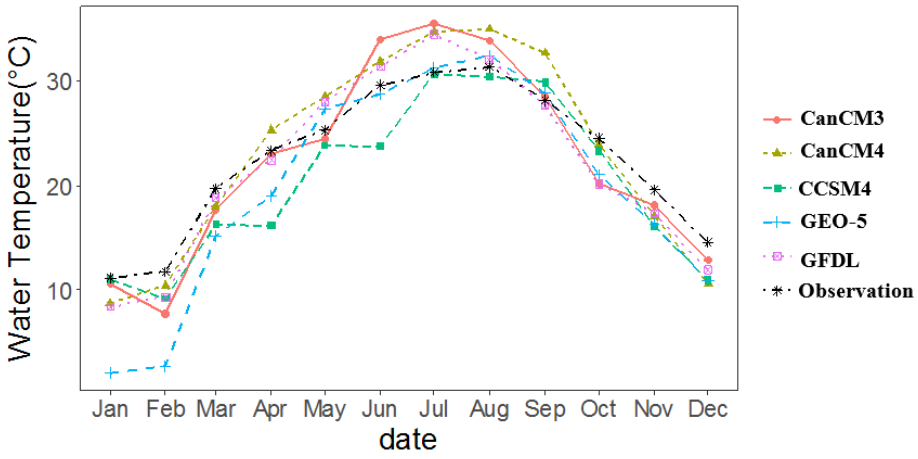

Figure 22. Water temperature predictions estimated from NMME seasonal air temperature.

The multi-regression based prediction model (as described in Task 4 deliverables) was then used to calculate the Chlorophyll-a concentrations from each of the five climate models. Figure 23 suggests that the results are very similar, except for those from GEO-5. This is because GEO-5

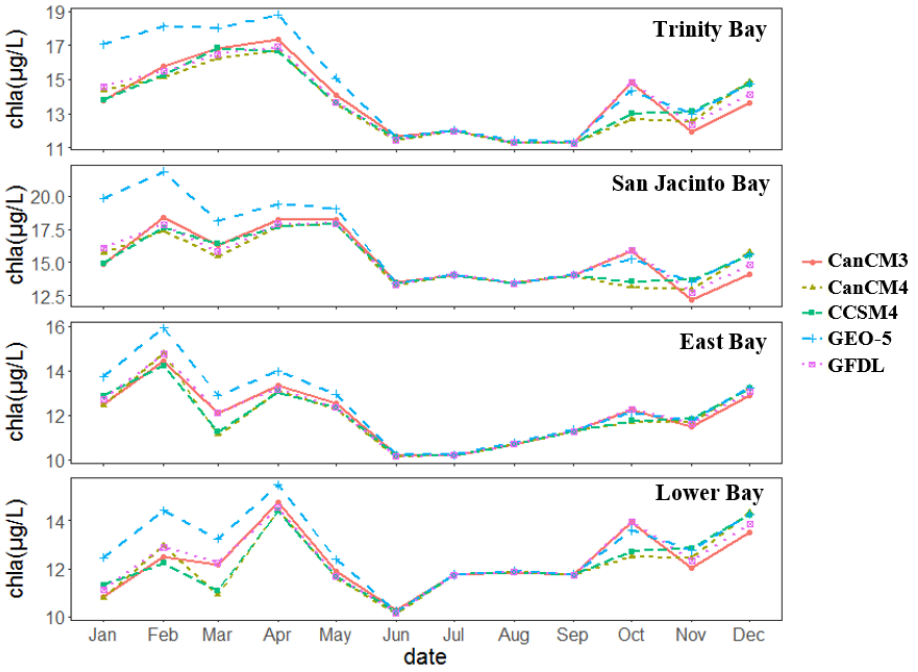

Figure 23. Predicted Chlorophyll-a concentrations using outputs from the five NMME models.

overestimated the river discharge significantly (Figure 20).

Considering the discrepancies among the climate models, a common practice is to use the ensemble mean for the final forecast. The results validation was conducted in two steps. First, the predicted-predicted (PP) Chlorophyll-a concentrations—which are the predicted concentrations when the empirical model is driven by the NMME-DHSVM predicted river discharge—were evaluated by the observations (i.e., the remotely sensed Chlorophyll-a product). Second, the PP results were further compared with the predicted-observed (PO) Chlorophyll-a concentrations—which are the predicted concentrations when the empirical model is driven by the observed river discharge. Results in Table 8 and Figure 24 suggest that the NMME-DHSVM predicted river discharge is the primary source of error. The Trinity and San Jacinto Bays have the largest errors during the growing season.

Table 8. Error statistics of the validation results

	Trinity Bay		**San Jacinto Bay**		**East Bay**		**Lower Bay**	
	PP	PO	PP	PO	PP	PO	PP	PO
MAE(µg/L)	1.49	0.62	1.42	0.8	1.06	0.66	1.07	1.02
RMSE(µg/L)	1.93	0.78	1.8	0.84	1.04	0.84	1.41	1.12
R^2	0.2	0.93	0.53	0.66	0.83	0.66	0.04	0.37

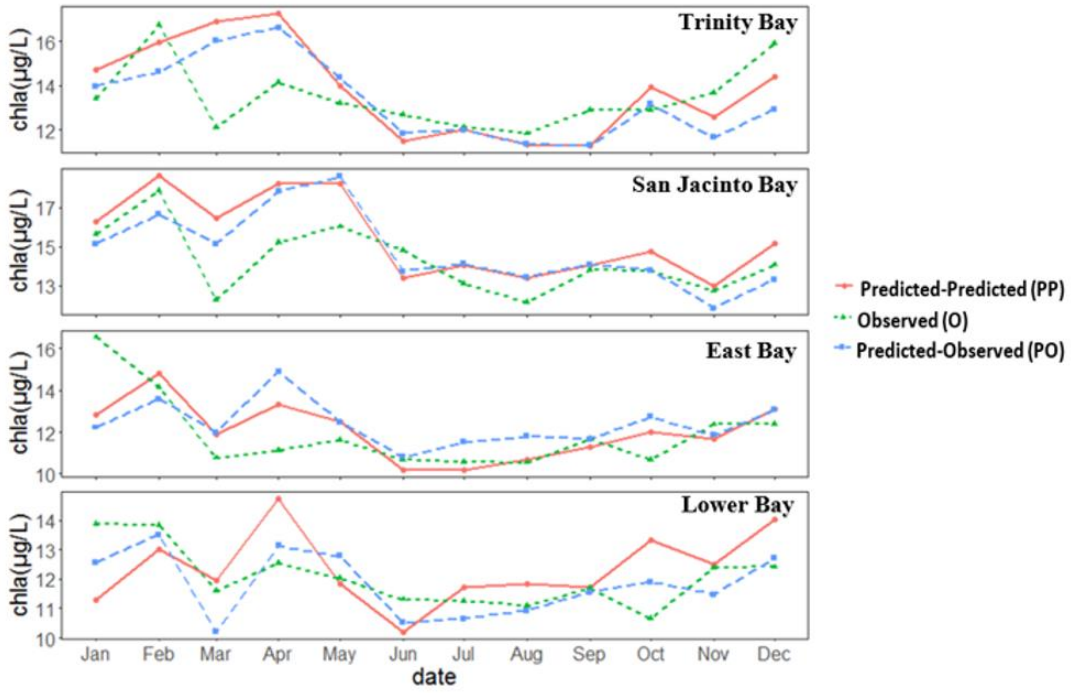

Figure 24. Validation of the ensemble mean of the predicted Chlorophyll-a concentrations. Red (Predicted-Predicted) is the modeled Chlorophyll-a using the predicted river discharge and water temperature; green (Observed) is the observed Chlorophyll-a from MERIS; and blue (Predicted-Observed) is the predicted Chlorophyll-a from observed variables.

8. Education, outreach, and publications

8.1.Education and outreach activities for high school students

The PI has been working with Mr. Luis Rivera—a high school teacher from San Antonio—through the Texas A&M Enrichment Experiences in Engineering (E3) RET program over the past 2.5 years. A "hands-on", activity based, environmental sustainability curricula was taught by Mr. Rivera successfully. Additionally, the high school students in Mr. Rivera's class have been collecting rainfall measurements using the rain gauges from this project. Mr. Rivera visited the PI's group for a week during the summers of 2016 and 2017 to improve his curricula. In addition, the PI's group also guided high school students in building sandbox modules during the "Camp BUILD" event here at Texas A&M—a one-week summer camp designed for

high school juniors and seniors (hosting 40 students per year), organized by the PI's home department (Civil Engineering).

8.2.Education and outreach activities for undergraduate and graduate students

PI Gao has mentored two undergraduate students through the College of Engineering's Undergraduate Summer Research Grant (USRG) program here at Texas A&M University. Mary Leece, from Baylor University, worked at the PI's lab for two months in 2016 and presented a poster on the discharge-chla relationship over Galveston Bay at the USRG forum. Carter Nickelson, from Whitworth University, worked on the discharge-chla relationship over Matagorda Bay in the summer of 2017.

Three graduate students—Zhang, Zhao and Shen—have been supervised and involved in this project. Zhang contributed to the remote sensing component, while Zhao worked on the DHSVM model calibration, validation, and streamflow prediction. Shen focused on developing the chla prediction model using a multi-regression approach, which led to his Master's thesis (defended on 9/7/17). Zhang and Zhao were trained to work as Teaching Assistants for the PI's courses (Remote Sensing in Hydrology, and Engineering Surface Water Hydrology) during the spring semester. Shen won the Water Daze Poster Competition award in 2016. Presentations and publications related to this project are listed in Section 8.4.

The PI used the remote sensing of chla concentration results in her "Remote Sensing in Hydrology" graduate course (CVEN602) to explain water quality monitoring. In the spring semesters of 2016 and 2017, a total of 30 graduate students from 7 different departments and programs at TAMU took this course.

8.3.Other outreach activities

In October 2016, PI Gao and Co-PI Roelke gave a presentation (entitled "Freshwater Inflows, Phytoplankton Productivity, and Coastal Ecosystem Sustainability – a Modeling and Remote Sensing Perspective") to the Galveston Bay Area Master Naturalist Chapter at the AgriLife Building in Carbide Park (in La Marque). This presentation was very well received by the audience, and the PI and co-PI had good interactions with the meeting participants afterward. In May 2017, PI Gao presented this research to the Texas Water Development Board (TWDB) and received positive feedback.

8.4.Presentations and Publications (indicate students)*

The following presentations and publications were generated from this project.

1. Gao, H., D. Roelke, A. Quigg, J. Gunn, S. Zhang*, G. Zhao*, and X. Shen*, Towards Monitoring and Predicting Phytoplankton Productivity over Galveston Bay: Some Preliminary Results, State of the Bay Symposium, Galveston, TX, 2016.
2. Zhang, S. *, H. Gao and D. Roelke, Monitoring Spatial-Temporal Variations of Chlorophyll-a in Galveston Bay, State of the Bay Symposium, Galveston, TX, 2016.
3. Zhang, S.*, H. Gao, A. Quigg and D. Roelke, Remote Sensing of Spatial-Temporal Variations of Chlorophyll-a in Galveston Bay, Texas, IEEE International Geoscience and Remote Sensing Symposium, 2016. (conference proceeding)
4. Shen, X*, H. Gao, S. Zhang, and K. Park, Potential impact of freshwater inflows on Chlorophyll a in a shallow estuary: a case study in Galveston Bay, Texas, Asia Oceania Geoscience Society Annual Meeting, 2016.

5. Shen, X*, Chlorophyll-a concentrations affected by freshwater inflow and climate conditions in Galveston Bay, Texas. M.S. Thesis, Texas A&M University, 2017.

Acknowledgement

We are thankful to Dr. Antonietta Quigg (Texas A&M University, Galveston (TAMUG)) for sharing the in-situ Chlorophyll-a data and Dr. Keyong Parker from (TAMUG) for some early discussions about the hydrodynamics.

References

Bricker, S. B., et al. (2008). "Effects of nutrient enrichment in the nation's estuaries: A decade of change." Harmful Algae **8**(1): 21-32.

Camacho, R. A., et al. (2015). "Modeling the Factors Controlling Phytoplankton in the St. Louis Bay Estuary, Mississippi and Evaluating Estuarine Responses to Nutrient Load Modifications." Journal of Environmental Engineering **141**(3).

Cloern, J. E. (1991). "Annual Variations in River Flow and Primary Production in the South San-Francisco Bay Estuary (USA)." Estuaries and Coasts : Spatial and Temporal Intercomparisons: 91-96.

Cloern, J. E. (2001). "Our evolving conceptual model of the coastal eutrophication problem." Marine Ecology Progress Series **210**: 223-253.

Froneman, P. W. (2002). "Response of the plankton to three different hydrological phases of the temporarily open/closed Kasouga estuary, South Africa." Estuarine Coastal and Shelf Science **55**(4): 535-546.

Harding, L. W. (1994). "Long-Term Trends in the Distribution of Phytoplankton in Chesapeake Bay - Roles of Light, Nutrients and Streamflow." Marine Ecology Progress Series **104**(3): 267-291.

Harding, L. W., Jr., et al. (2016). "Variable climatic conditions dominate recent phytoplankton dynamics in Chesapeake Bay." Sci Rep **6**: 23773.

Le, C., et al. (2016). "Bio-optical water quality dynamics observed from MERIS in Pensacola Bay, Florida." Estuarine, Coastal and Shelf Science **173**: 26-38.

Livneh, B., et al. (2013). "A Long-Term Hydrologically Based Dataset of Land Surface Fluxes and States for the Conterminous United States: Update and Extensions." Journal of Climate **26**(23): 9384-9392.

Malone, T. C., et al. (1988). "Influences of River Flow on the Dynamics of Phytoplankton Production in a Partially Stratified Estuary." Marine Ecology Progress Series **48**(3): 235-249.

Meybeck, M., et al. (1988). "Nutrients (Organic C, P, N, Si) in the Eutrophic River Loire (France) and Its Estuary." Estuarine Coastal and Shelf Science **27**(6): 595-624.

Miller, W. D. and L. W. Harding (2007). "Climate forcing of the spring bloom in Chesapeake Bay." Marine Ecology Progress Series **331**: 11-22.

Ornolfsdottir, E. B., et al. (2004). "Nutrient pulsing as a regulator of phytoplankton abundance and community composition in Galveston Bay, Texas." Journal of Experimental Marine Biology and Ecology **303**(2): 197-220.

Roberts, A. D. and S. D. Prince (2010). "Effects of urban and non-urban land cover on nitrogen and phosphorus runoff to Chesapeake Bay." Ecological Indicators **10**(2): 459-474.

Roelke, D. L., et al. (2013). "Co-occurring and opposing freshwater inflow effects on phytoplankton biomass, productivity and community composition of Galveston Bay, USA." Marine Ecology Progress Series **477**: 61-76.

Shen, X, et al. (2016). "Potential impact of freshwater inflows on Chlorophyll a in a shallow estuary: a case study in Galveston Bay, Texas." Asia Oceania Geoscience Society Annual Meeting.

Xia, M. and L. Jiang (2015). "Influence of wind and river discharge on the hypoxia in a shallow bay." Ocean Dynamics **65**(5): 665-678.

Zhang, S., et al. (2016). "Remote Sensing of Spatial-Temporal Variations of Chlorophyll-a in Galveston Bay, Texas." 2016 Ieee International Geoscience and Remote Sensing Symposium (Igarss): 5841-5844.

Zhao, G., et al. (2016). "Integrating a reservoir regulation scheme into a spatially distributed hydrological model." Advances in Water Resources **98**: 16-31.